18TH WORLD CONFERENCE ON EARTHQUAKE ENGINEERING
WCEE2024
MILAN

MILAN, ITALY
30TH JUNE - 5TH JULY 2024

www.wcee2024.it

SIMULATED GROUND-MOTION RECORDS FOR THE SEISMIC ASSESSMENT OF MONUMENTAL MASONRY STRUCTURES

Shaghayegh Karimzadeh[1], Marco F. Funari[2], Simon Szabó[1], S. M. Sajad Hussaini[1], Sanaz Rezaeian[3], Paulo B. Lourenço[1]

[1]Department of Civil Engineering, Institute for Sustainability and Innovation in Structural Engineering (ISISE), Advanced Production and Intelligent Systems (ARISE), University of Minho, Guimarães, Portugal.

[2]School of Sustainability, Civil and Environmental Engineering, University of Surrey, Guildford, UK.

[3]U.S. Geological Survey, Golden, CO, USA.

Corresponding author's email: shaghkn@civil.uminho.pt

Abstract: *Earthquakes are natural hazards that can cause widespread devastation and loss of life. Simulated ground-motion records can be useful in regions with limited seismic stations or a history of damaging but infrequent earthquakes. This is especially true in areas with a high concentration of heritage masonry structures, which are especially susceptible to damage, as simulated records can be crucial in predicting their seismic response. Despite the importance of simulated earthquakes, few studies have investigated how effective they are compared to real earthquakes when assessing the structural response of heritage buildings. To address this knowledge gap, we use two different simulation methods of the moment-magnitude 6.2 Faial earthquake, which occurred on July 9, 1998, in the Azores, to replicate the recorded time-series at four available stations within an epicentral distance of 150 km. The study has two objectives: first, to validate the simulated records of the 1998 Faial earthquake using alternative stochastic ground-motion simulation approaches, and second, to determine how these approaches affect the seismic assessment of historic monumental masonry structures. To accomplish these objectives, this study uses real and simulated ground-motion datasets to conduct non-linear response history analyses of the São Francisco Church, a structure in Horta that sustained damage during the Faial earthquake. The results show that both simulation approaches yield structural responses similar to those from the observed records.*

Keywords: Monumental Masonry Structures, Non-linear Response History Analysis, Ground Motion Simulation, Stochastic Source-Based Approach, Stochastic Site-Based Approach, 1998 Faial Earthquake (Azores)

1. Introduction

Recent events, especially the 2023 earthquakes in Turkey, have shown that earthquakes are among the most destructive natural hazards, resulting in fatalities and substantial structural damage and failures. Monumental masonry structures, particularly in the absence of box-like or integral structural behavior, are prone to experience out-of-plane (OOP) failure mechanisms (Funari, Mehrotra and Lourenço, 2021; Stepinac et al.,

2021; Funari, Mehrotra and Lourenço, 2021; Stepinac et al., 2021), resulting in the loss of artistic and historical assets and, at the same time, immaterial loss of memory and people's identity.

To define a strategy for architectural heritage conservation, one can refer to studies from the U.S. National Institute of Building Sciences (NIBS) that show the investment in mitigation saves six times the amount for damage repair ("prevention pays") (*Home | National Institute of Building Sciences*, 27 August 2021). Recent applications of computational methods such as the finite-element method (FEM) (Valente and Milani, 2016; Fortunato, Funari and Lonetti, 2017; Funari, Hajjat, *et al.*, 2021; Funari, Silva, *et al.*, 2021; Marco F Funari *et al.*, 2022) and discrete element method (DEM) (Gobbin, de Felice and Lemos, 2021; Marco Francesco Funari *et al.*, 2022; Pulatsu *et al.*, 2022) offer avenues for assessing seismic vulnerability by modeling the masonry material using different representation scales. Both macro- and micro-modeling are suitable for performing seismic assessment of masonry structures. The macro-modeling strategy is an efficient solution that addresses the computational challenges posed when one wants to perform non-linear response history analysis (NLRHA) of large-scale masonry structures. In this case, the full time-series of ground motion records are required. However, they are not always available, particularly in regions lacking seismic stations. To address this limitation, ground-motion simulations offer reliable solutions such as deterministic source-based, stochastic source-based, stochastic site-based, and hybrid models (Rezaeian and Xiaodan, 2014). Stochastic methods are favored in engineering applications due to their simplicity and practicality, as they do not necessitate intricate modeling input details. They are particularly valuable after parameter calibration for specific regions. Yet, it is crucial to validate these simulations before using them in engineering contexts (Burks, 2014; Atkinson and Assatourians, 2015; Karimzadeh *et al.*, 2020; Can, Askan and Karimzadeh, 2021; Karimzadeh and Lourenço, 2021).

Our study compares ground motions generated by a stochastic source-based model (Assatourians and Atkinson, 2012) and a stochastic site-based model (Rezaeian and der Kiureghian, 2008). We simulate ground-motion data recorded during the 1998 moment magnitude (M_w) 6.2 Faial earthquake event, assessing four stations with epicentral distances under 150 km. The modeling input parameters for both approaches are calibrated to ensure accurate simulation results. We use goodness-of-fit (GOF) scores (Olsen and Mayhew, 2010) to evaluate the simulations. Differences between the observed and synthetic ground-motion datasets are also assessed by using as a structural benchmark: the São Francisco Church in Horta, which suffered damage during the 1998 Faial earthquake.

2. Study Area

The Azores plateau is positioned at the convergence of three major tectonic plates: North America, Eurasia, and Nubia (Figure 1) (Lourenço *et al.*, 1998). This plateau encompasses several islands, including Faial, Pico, São Jorge, São Miguel, Santa Maria, Graciosa, and Terceira, which have experienced destructive earthquakes over the years (Gaspar *et al.*, 2015). Notable historical seismic events include the 1926 body-wave magnitude (M_b) ~5.6 earthquake, the 1958 earthquake registering a maximum modified Mercalli intensity (MMI_{max}) of X, and the 1998 M_w 6.2 earthquake, which impacted Faial Island (Lourenço *et al.*, 1998; Matias *et al.*, 2007; Carvalho, Reis and Vales, 2016).

The 1998 Faial earthquake had widespread impacts on structures and was felt across nearly all the Azores region. The earthquake resulted in substantial structural damage, particularly on the Faial and Pico islands, reaching an MMI_{max} of VIII (Matias *et al.*, 2007). The event led to 8 reported fatalities, with 150 individuals sustaining injuries, and 1500 left homeless. Furthermore, approximately 2100 buildings partially or completely collapsed (Senos *et al.*, 1998). This earthquake was recorded at five ground-motion stations, as listed in **Error! Reference source not found.**. The table provides data on the epicentral distance (R_{epi}), along with the peak ground acceleration (PGA) and peak ground velocity (PGV), for both the east-west (EW) and north-south (NS) directions.

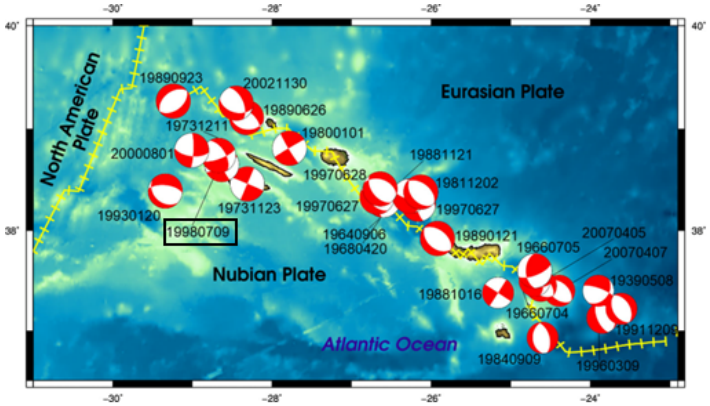

Figure 1. Geospatial representation of 26 seismic events > M_w 5.0 in the Azores region from 1939 to 2007. Active spreading centers are highlighted with yellow lines, and the black box identifies the 1998 Faial event. The fault mechanism is represented by the beachballs. The dates for each event are provided in black text, formatted as YYYYMMDD. Figure adapted from (Carvalho, Reis and Vales, 2016).

Table 1. Details of the five stations with recorded data from the 1998 Faial earthquake.

Station Code	Latitude (°)	Longitude (°)	R_{epi} (km)	PGA-EW (cm/s^2)	PGA-NS (cm/s^2)	PGV-EW (cm/s)	PGV-NS (cm/s)
GZC	39.084	-28.006	72	17.0	14.6	1.0	1.0
PVI	38.726	-27.057	132	8.6	10.0	0.8	0.7
HOR	38.530	-28.630	11	434.5	424.0	29.3	37.9
MOS	37.892	-25.822	254	4.1	5.1	0.2	0.2
SEB	38.668	-27.088	129	17.5	21.2	1.4	2.2

3. Ground motion simulation

3.1. Source-based stochastic approach

The stochastic source-based methods include both point-source and finite-fault techniques for modeling ground motion at selected stations. The original version was a point-source approach, which was initially presented by Boore (1983). This current study uses the stochastic finite-fault ground motion simulation methodology, implemented through the EXSIM12 platform (Assatourians and Atkinson, 2012), to model the acceleration time-series of the scenario event. The simulation algorithm proposed by Motazedian and Atkinson (2005), based on the FINSIM code by Beresnev and Atkinson (1998), is improved with the suggestions of Boore (2009). This approach considers multiple factors to identify the fault rupture, including earthquake magnitude, fault geometry, slip distribution, crustal density, rupture velocity, and strike. The method combines the source contribution with attenuation parameters and site effects to obtain the seismic signal in the time domain at any observation site.

In the stochastic finite-fault method, the ruptured fault plane is divided into smaller sub-sources represented as a grid, with each sub-source assumed to be a point-source with a ω^{-2} source spectrum of acceleration. The sub-sources rupture with a time delay that depends on their distance from the hypocenter, and the time-domain summation of the contributions from the delayed sub-sources is carried out to obtain the final ground-motion record (Motazedian and Atkinson, 2005).

Earlier research conducted in the Azores region has brought attention to a variety of seismic sources and attenuation models (Olafsson, Sigbjörnsson and Einarsson, 1998; Zonno *et al.*, 2010; Marques *et al.*, 2014; Carvalho, Reis and Vales, 2016). This study adopts the region-specific input parameters suggested by Carvalho, Reis and Vales (2016) and subsequently validated by (Karimzadeh and Lourenço, 2021; Karimzadeh *et al.*, 2023, 2024) to simulate the data recorded at the chosen four stations within an epicentral distance of 150 km. It is worth noting that these parameters were validated against the ground-motion records from the 1998 Faial earthquake, demonstrating a high level of accuracy as evidenced by the evaluation of GOF scores. The results are discussed in Section 3.3.

3.2. Site-based stochastic approach

This study also uses the stochastic site-based model proposed by Rezaeian and der Kiureghian (2008). The model is based on modulating a filtered white-noise process. The modulation accounts for temporal non-stationarity, while filtering is based on a time-variant system that accounts for spectral non-stationarity. The model aims to represent essential characteristics of a recorded ground motion using a fitting procedure instead of modeling the earthquake source rupture, path effects, and site characteristics. The form of the model is expressed as follows:

$$x(t) = q(t,\alpha)\left\{\frac{1}{\sigma_h(t)}\int_{-\infty}^{t} h(t-\tau,\lambda(\tau))\cdot w(\tau)d\tau\right\} \quad (1)$$

where $x(t)$ is the acceleration time-series, $q(t,\alpha)$ is a deterministic time modulation function, $h(t-\tau,\lambda(\tau))$ is the impulse response function of the filter, $w(\tau)$ is the white-noise process, and $\sigma_h(t)$ is the standard deviation of the integral process. Following Rezaeian and der Kiureghian (2008), the pseudo spectral acceleration response of a single-degree-of-freedom system is used for the filter function. A piece-wise constant and a linear function are used for the variation of the damping ratio and natural frequency parameters, respectively:

$$\zeta_f(\tau) = \begin{cases} \zeta_1, & \text{if } 0 < \tau \le T_{\zeta_1} \\ \zeta_2, & \text{if } T_{\zeta_1} < \tau \le T_{\zeta_2} \\ \zeta_3, & \text{if } T_{\zeta_2} < \tau \le t_n \end{cases} \quad (2)$$

$$\omega_f(\tau) = \omega_0 - (\omega_0 - \omega_n)\cdot\frac{\tau}{t_n} \quad (3)$$

where ζ_1, ζ_2, and ζ_3 are constant damping ratios, T_{ζ_1} and T_{ζ_2} are the times at which the damping ratios change, t_n is the total duration of motion, and ω_0 and ω_n are the initial and final frequency, respectively. The temporal variation of the waveform uses a piece-wise time modulation as follows:

$$q(t) = \begin{cases} 0, & \text{if } t \le T_0 \\ \alpha_1\left(\dfrac{t-T_0}{T_1-T_0}\right)^2, & \text{if } T_0 < t \le T_1 \\ \alpha_1, & \text{if } T_1 < t \le T_2 \\ \alpha_1\cdot e^{\left[-\alpha_2\cdot(t-T_2)^{\alpha_3}\right]}, & \text{if } T_2 < t \end{cases} \quad (4)$$

where T_0 is the start time of process, and T_1 and T_2 are the start and end of the strong-motion phase, respectively. α_1 denotes the intensity of the strong-shaking phase, while α_2 and α_3 are the shape parameters of the function.

Following the objective functions in Rezaeian and der Kiureghian (2008), here the six time-modulation function parameters are identified by matching the cumulative expected energy of the stochastic process with that of each recorded ground motion. Similarly, the seven parameters of the filter function are identified by fitting the cumulative expected number of zero-level up-crossings of the stochastic process and the average cumulative number of positive minima and negative maxima of 10 simulated processes to those of each recorded ground motion. Table 2 shows the identified model parameters of the site-based stochastic model.

Table 2. Identified model parameters of the stochastic site-based ground-motion simulation approach.

Station	Component	α_1	α_2	α_3	T_0	T_1	T_2	ω_0	ω_n	ζ_1	ζ_2	ζ_3	$T_{\zeta 1}$	$T_{\zeta 2}$
GZC	EW	0.0631	0.293	0.572	29.0	33.0	33.6	25.66	1.00	0.30	0.10	0.6	30.0	43.0
	NS	0.0523	0.338	0.535	29.0	33.0	33.5	19.90	0.25	0.40	0.15	0.5	33.0	45.0
PVI	EW	0.0324	0.305	0.517	32.9	35.0	41.3	16.10	0.27	0.10	0.10	0.6	45.0	48.0
	NS	0.0300	0.232	0.541	32.8	35.0	39.9	18.48	0.48	0.13	0.20	0.4	40.0	50.0
HOR	EW	1.8930	0.468	0.684	0.8	3.9	4.5	37.42	6.00	0.30	0.80	0.9	2.5	7.0
	NS	1.5550	0.715	0.264	0	3.9	5.3	41.94	4.94	0.40	0.80	0.4	3.0	7.0
SEB	EW	0.0598	0.151	0.609	28.0	32.1	39	17.81	0.58	0.20	0.12	0.9	35.0	58.0
	NS	0.0790	0.392	0.401	28.0	31.6	40.8	16.48	0.57	0.20	0.20	0.4	35.0	55.0

3.3. Simulation results

In this section, we compare the observed and simulated time-series using the GOF validation approach (Olsen and Mayhew, 2010). We validate the simulated records of the 1998 Faial earthquake using a suite of seismological measures, including PGA, PGV, peak ground displacement (PGD), PGV/PGA ratio, Arias intensity, cumulative absolute velocity, acceleration spectrum intensity, modified acceleration spectrum intensity for the period range of 0.1 to 2.5 seconds (Yakut and Yılmaz, 2008), velocity spectrum intensity, Housner intensity, bracketed duration, Fourier amplitude spectrum (FAS) within the frequency range of 0.1 to 25 Hz, and pseudo-spectral acceleration (PSA) within the period range of 0 to 4 seconds using a 5% damping ratio. The fit is categorized as follows: 80–100 as an excellent fit, 65–80 as a very good fit, 45–65 as a fair fit, 35–45 as a poor fit, and less than 35 as a bad fit (Olsen and Mayhew, 2010).

Figure 2 and Figure 3 present the results for observed ground motion records alongside synthetic motions from both stochastic approaches, including full time-series, FAS, and PSA at the selected four stations. Station HOR has the shortest source-to-site distance and recorded ground-motion duration among these stations. With an epicentral distance of 11 km, this near-field station recorded a maximum horizontal PGA of 434.5 cm/s^2. The simulated PGA values from the source-based and site-based approaches are estimated as 417.0 cm/s^2 and 488.0 cm/s^2 (maximum of EW and NS components), respectively. Overall, the spectral characteristics of the simulated motions closely match the observed records in the frequency range of 0.1–25 Hz. Station GZC recorded a PGA of 17.0 cm/s^2, while the source-based and site-based methods simulated PGA values of 16.0 cm/s^2 and 15.0 cm/s^2, respectively. The source-based simulation slightly overestimates the FAS in the 0.4–1.0 Hz frequency band, which is also evident in the spectral ordinates. At station SEB, a far-field station with the largest epicentral distance, the observed PGA is 21.2 cm/s^2, while the source-based and site-based methods yield PGA values of 11.0 cm/s^2 and 22.0 cm/s^2, respectively. The simulated FAS from the source-based approach underestimates observations for frequencies above 1.0 Hz. This underestimation of low-period content may be due to inadequate modeling of soil effects at this site. Moreover, the observed PSA at station SEB exhibits multiple dominant periods that are not adequately captured by the single-mode filter used in the site-based method, reflecting a limitation of this approach. Finally, station PVI recorded a PGA of 10.0 cm/s^2, and both stochastic simulations resulted in a PGA of 8.0 cm/s^2. The simulated FAS closely resembles the real FAS, except for a slight overestimation of the amplitude at frequencies below 1.0 Hz, which is evident in the PSA.

Table 3 presents GOF scores derived from both simulation approaches at the stations. The source-based stochastic method's simulations are assessed by comparing them to the geometric mean of the observed horizontal components. The GOF scores for the source-based approach at the stations consistently achieve high scores, indicating very good fits. These simulations closely resemble observed records across various seismological aspects, except for the simulated time-series at station SEB, which shows a fair fit.

We conduct a component-wise comparison for the site-based stochastic simulations, evaluating each direction individually. The GOF scores for these simulations consistently indicate an excellent fit with the observed records for all stations and components, with minor exceptions for the EW component at station GZC and the NS component at station HOR. Because the site-based approach relies on a fitting procedure to replicate recorded motion characteristics, these deviations were expected. In terms of average PGA, we observed that

the synthetic ground motions from the site-based method were, on average, 10.4% higher, while those from the source-based method were, on average, 6.4% lower than recorded motions.

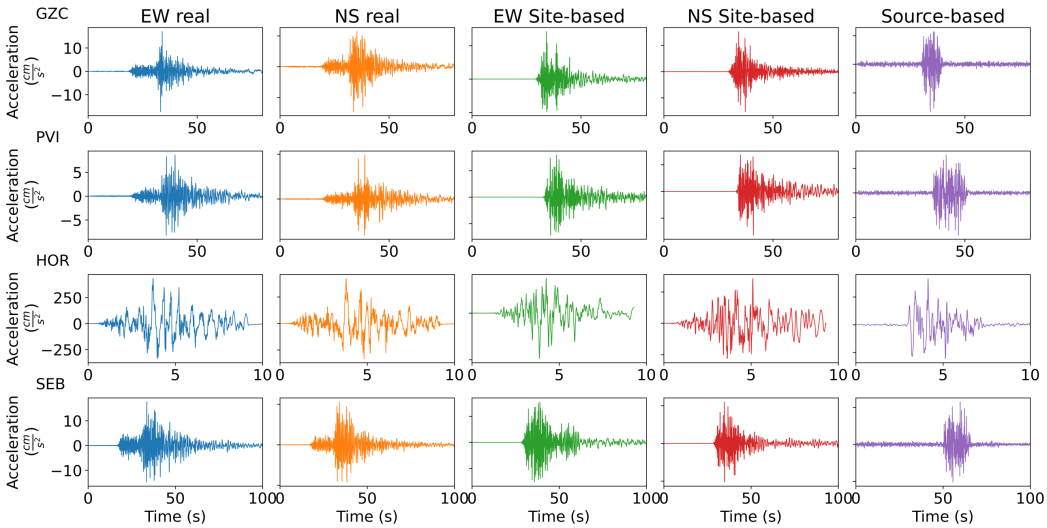

Figure 2. Real and simulated time-series at stations GZC, PVI, HOR, and SEB for the East-West (EW) and North-South (NS) components.

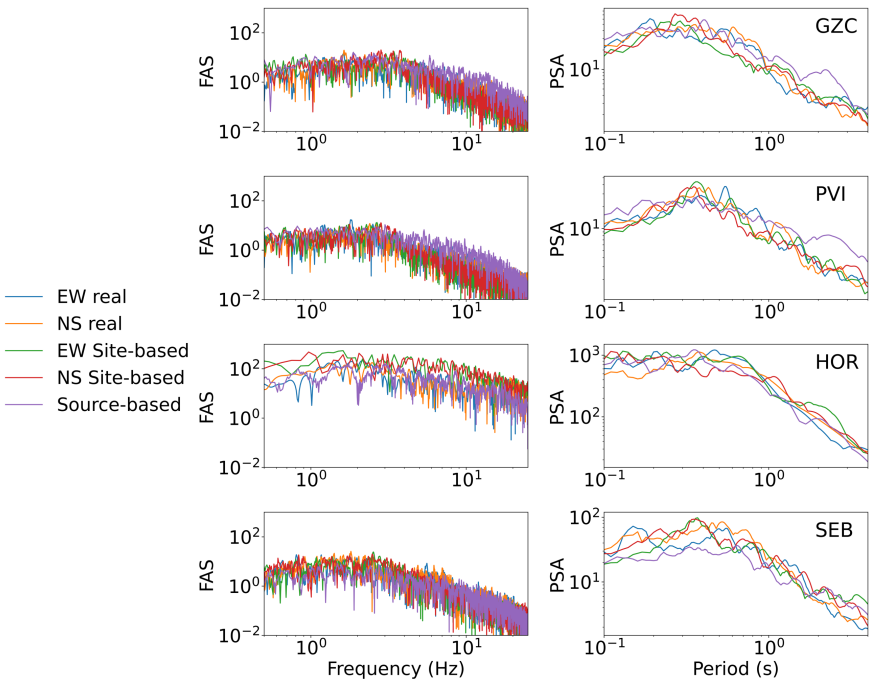

Figure 3. Real and simulated Fourier amplitude spectrum (FAS) and pseudo-spectral acceleration (PSA) at stations GZC, PVI, HOR, and SEB for the East-West (EW) and North-South (NS) components of the records.

Table 3. Goodness-of-fit (GOF) scores for real and simulated ground motion records of the 1998 Faial earthquake (moment magnitude (M_w) 6.2) for the East-West (EW) and North-South (NS) components.

Station	Source-based		Site-based		
	GOF	Fit Category	Direction	GOF	Fit Type
GZC	68	Very good	EW	77	Very good
			NS	81	Excellent
PVI	67	Very good	EW	84	Excellent
			NS	84	Excellent
HOR	72	Very good	EW	81	Excellent

			NS	79	Very good
SEB	57	Fair	EW	80	Excellent
			NS	83	Excellent

4. Structural Modeling

4.1. Numerical finite-element modeling

In this work, we use a macro-modeling approach in which the masonry arrangement is smeared over a homogeneous material. This is particularly convenient for the analysis of large-scale structures because it offers the possibility of reproducing the macroscopic masonry mechanical behavior through several models (e.g., the smeared crack concrete, brittle crack concrete, and concrete damage plasticity (CDP) models). Specifically, CDP couples plasticity with a scalar-based damage model, and, because it was originally developed for concrete, an isotropic elastic behavior is assumed (Lubliner *et al.*, 1989). This is a limitation when adapting CDP to masonry, as material orthotropy may have an important role, especially when periodic or non-periodic masonry arrangements are present.

The quasi-brittle nature of masonry is represented by linear softening. Damage variables are used to reduce the initial (undamaged) elastic modulus when softening is active. Damping is another important factor that influences the seismic performance of masonry structures. For historic masonry buildings, the damping ratio value ranges between 3% (Formisano *et al.*, 2021) and 5% (Hoveidae, Fathi and Karimzadeh, 2021). We use the Rayleigh damping model, which approximates the damping coefficient as a linear combination of mass and stiffness.

The three-dimensional (3D) FE model necessitates the use of solid elements; therefore, the mesh discretization is achieved using 3D tetrahedron (Delaunay) FEs, due to their adaptability to more complex geometries. The TETC3D4 FEs in ABAQUS CAE (Abaqus, 2014), based on a tetrahedral geometry with linear shape functions, have been used. Furthermore, NLRHA is performed by applying a real or simulated record. The loading is separated into two stages: gradual application of gravity loads and, subsequently, the ground-motion record, which is applied to the base of the structure along the two principal geometrical directions, namely X and Y. To integrate the equations of motion, we use an implicit time-integration scheme with non-linear geometric effects taken into consideration (Abaqus, 2014).

4.2. Comparison framework

Beyond a reliable FEM to perform high-fidelity NLRHAs, an appropriate comparison framework that considers several structural response measures (SRM) needs to be defined. This subsection briefly describes the methodologies used to treat the SRMs obtained by simulating the seismic behavior of the masonry structure via both observed and simulated (i.e., source-based and site-based) ground motions. Relative errors in the prediction of SRMs are calculated with respect to the response obtained with the observed ground motion. We consider the following response measures:

- Maximum base shear
- Maximum horizontal displacement (a control-point network is considered)

The selection of base shear and displacement as response measures is a common engineering approach to assess seismic performance according to force or displacement capacities.

The relative errors in the considered response measures are computed with the following equations:

$$RE = \frac{Test\ B - Test\ A}{Test\ A} \tag{5}$$

where $Test\ B$ and $Test\ A$ refer to a specific SRM obtained using simulated and real records, respectively.

5. Results of Response History Analysis

The real and simulated ground-motion datasets are used to perform NLRHA of the São Francisco Church, located at Horta. The 3D analysis was performed using a detailed geometrical survey commissioned by the authors. The geometrical model of the São Francisco Church and the nomenclature of the control points monitored (1 to 9) are presented in (

Figure 4).

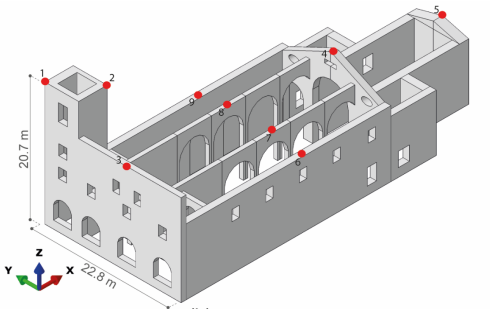

Figure 4. Geometry and control points of the São Francisco Church.

As mentioned earlier, the CDP model is used to model the non-linear behavior of the masonry material. The elastic behavior is described by the elastic modulus and the Poisson ratio, which are set equal to 1.0 GPa and 0.2, respectively. Even if out of the scope of this paper, the damping factor has been calibrated such that the damage of the numerical model is reasonably close to that surveyed post-earthquake in 1998. Precisely, the damping ratio was calibrated as equal to 5%. The other mechanical parameters are detailed in Table 4 and

Table 5. There, d_c and d_t denote the compressive and tensile damage parameters, respectively, while f_{b0}/f_{c0} signifies the ratio of initial equibiaxial compressive yield stress to initial uniaxial compressive yield stress, and K_c signifies the ratio of the second stress invariant on the tensile meridian to that on the compressive meridian.

Table 4. Compressive and tensile behavior of the masonry. d_c and d_t are the compressive and tensile damage parameters, respectively.

Compressive behavior			Tensile behavior		
Stress [MPa]	Inelastic strain	d_c	Stress [MPa]	Inelastic strain	d_t
2.20	0	0	0.150	0	0
2.60	0.005	0	0.001	0.003	0.9
0.20	0.012	0.9	0.001	0.010	0.9
0.20	0.020	0.9	-	-	-

Table 5. Drucker-Prager strength domain parameters. f_{b0}/f_{c0} is the ratio of initial equibiaxial compressive yield stress to initial uniaxial compressive yield stress; K_c is the ratio of the second stress invariant on the tensile meridian to that on the compressive meridian.

Dilatation angle	Eccentricity	f_{b0}/f_{c0}	K_c	Viscosity parameter
10°	0.1	1.16	2/3	0.002

One-dimensional NLRHAs have been performed by applying the ground motion in turn along the X and Y directions at both polarities. One can note that the far-field stations (GZC, PVI, SEB that are denoted as far-field 1, 2 and 3 in the following) have relatively low PGA, generating linear elastic responses of the masonry

structures. On the other hand, the near-field station (HOR) is characterized by a higher PGA, which is expected to generate damage. For the sake of comparison, the near-field records have also been used to run response history analyses with a linear elastic constitutive material relation to quantify how the appearance of damage affects the accuracy of the two investigated ground-motion simulation approaches; thus, the total number of NLRHAs performed is equal to 100. The results obtained by the source-based simulation approach have been used to compute two relative errors, one with respect to each component of the real records (NS and EW). On the other hand, the site-based relative errors have been computed with respect to the real component simulated.

Figure 5 and Figure 6 report the relative errors (obtained with the two simulated approaches) of control point displacements (RE_d) and base shear (RE_{SB}) with respect to the NLRHAs performed with the real ground motions. The first terms in the legend refer to the simulation approach (site- or source-based), while the second shows the component of the real record (EW or NS) with which it is compared. Considering the control point displacement predictions, the errors rarely exceed 50%, mainly in the near-field simulations considering a non-linear constitutive relation. However, such a result was expected because the material and geometrical non-linearities affect macro elements' local stiffness and increase the predicted error.

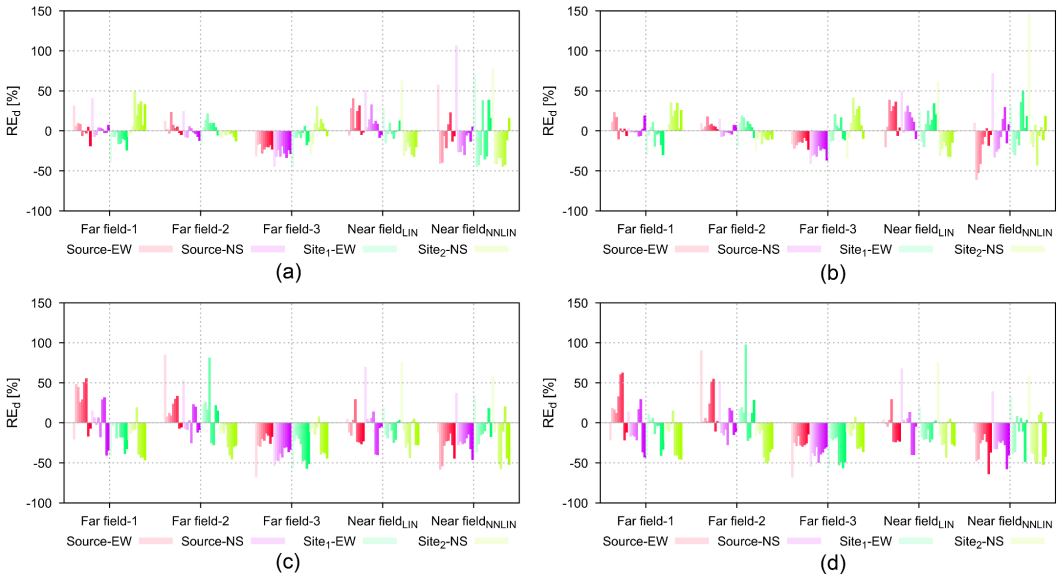

Figure 5. Relative error in maximum displacement (RE_d) for each control point: (a) +X, (b) -X, (c) +Y, (d) -Y for the East-West (EW) and North-South (NS) components of the records.

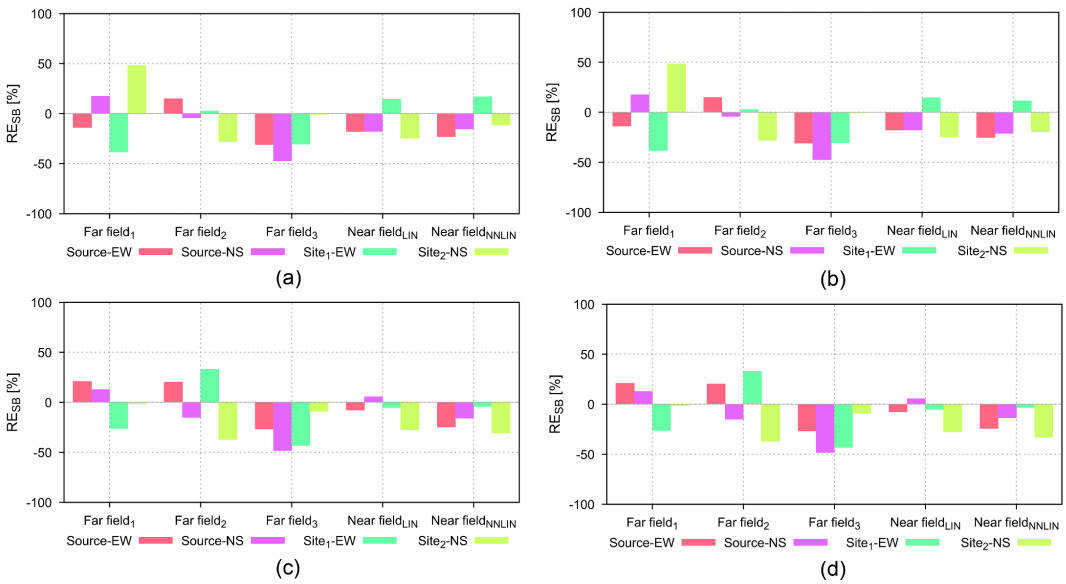

Figure 6. Relative error in maximum base shear (RE_{SB}): (a) +X, (b) -X, (c) +Y, (d) -Y for the East-West (EW) and North-South (NS) components of the records.

The comparison also confirms the same trend in base-shear prediction, where errors appear within a reasonable accuracy range. Regarding the near-field simulations, results show a pattern of underestimating the prediction, particularly when non-linear constitutive relations have been used.

6. Conclusions

This study aims to simulate the 1998 M_w 6.2 Faial earthquake using alternative stochastic ground-motion simulation methods and assess their effect on the dynamic response of a historic masonry structure. Both simulation approaches are calibrated and validated against recorded time-series data from the 1998 Faial earthquake at four available stations within an epicentral distance of 150 km.

The stochastic site-based approach outperforms the source-based approach, as evidenced by higher goodness-of-fit (GOF) scores. The source-based method requires more specific source, path, and site information, while the site-based approach is more practical and computationally efficient but relies on record-specific calibration. The site-based method produces similar GOF scores for both near-field and far-field stations, which may be attributed to its inherent fitting technique. Conversely, the source-based method exhibits the highest GOF score for the near-field station. The poorest match is observed at the farthest station, possibly due to inadequate attenuation or an unsuitable soil model. However, the source-based method results in GOF scores within a similar range for the remaining stations.

Errors observed from near-field site-based simulations in estimating maximum ground displacement are attributed to the neglect of correlations between components and the absence of directivity pulses in the model, which are important in near-fault motions. Directivity pulses stemming from fault rupture are not considered in the simulations and may contribute to errors. When predicting structural control point displacements, it is noteworthy that errors exceeding 50% are infrequent, mainly in near-field simulations involving non-linear constitutive relations. This outcome was anticipated, as material and geometric non-linearities affect the local stiffness of macro elements, increasing the predicted error. The comparison shows a consistent base-shear prediction pattern, with errors falling within an acceptable margin of accuracy, indicating excellent performance of the simulated ground motions. Notably, observations tend to be underestimated when focusing solely on near-field simulations, especially when using non-linear constitutive relations.

In conclusion, the simulation accuracy varies depending on the application, and further research is needed to explore the effects of correlations and directivity pulses, especially for near-field site-based simulations. This study motivates broader investigations involving a range of events, more near-field stations, and other structural types for seismic assessment.

7. Acknowledgements

This work was partly financed by FCT/MCTES through national funds (PIDDAC) under the R&D Unit ISISE under reference UIDB/04029/2020, and under the Associate Laboratory Advanced Production and Intelligent Systems ARISE under reference LA/P/0112/2020. This study has been partly funded by the STAND4HERITAGE project that has received funding from the European Research Council (ERC) under the European Union's Horizon 2020 research and innovation program (Grant agreement No. 833123), as an Advanced Grant. This work is also partly financed by MPP2030-FCT PhD Grants under the R&D Unit Institute for Sustainability and Innovation in Structural Engineering (ISISE), under reference PRT/BD/154348/2022. This work is partly financed by national funds through FCT - Foundation for Science and Technology, under grant agreement UI/BD/153379/2022 attributed to the 4th author.

8. Disclaimer

Any use of trade, firm, or product names is for descriptive purposes only and does not imply endorsement by the U.S. Government.

9. References

Abaqus, V. (2014). ‘6.14 Documentation’, *Dassault Systemes Simulia Corporation*, 651(6.2).

Assatourians, K. and Atkinson, G. (2012) 'EXSIM12: A Stochastic Finite-Fault Computer Program in FORTRAN'.

Atkinson, G.M. and Assatourians, K. (2015). 'Implementation and validation of EXSIM (a stochastic finite-fault ground-motion simulation algorithm) on the SCEC broadband platform', *Seismological Research Letters*, 86(1), pp. 48–60. doi: 10.1785/0220140097

Beresnev, I.A. and Atkinson, G.M. (1998). 'FINSIM--a FORTRAN program for simulating stochastic acceleration time histories from finite faults', *Seismological Research Letters*, 69(1), pp. 27–32. doi: 10.1785/gssrl.69.1.27

Boore, D.M. (1983). 'Strong-motion seismology', *Reviews of Geophysics*, 21(6), pp. 1308–1318. doi:10.1029/RG021i006p01308

Boore, D.M. (2009). 'Comparing stochastic point-source and finite-source ground-motion simulations: SMSIM and EXSIM', *Bulletin of the Seismological Society of America*, 99(6), pp. 3202–3216. doi:10.1785/0120090056

Burks, L.S. (2014). *Ground motion simulations: Validation and application for civil engineering problems*. Stanford University.

Can, G., Askan, A. and Karimzadeh, S. (2021). 'An assessment of the 3 February 2002 Cay (Turkey) earthquake (Mw= 6.6): Modeling of ground motions and felt intensity distribution', *Soil Dynamics and Earthquake Engineering*, 150, p. 106832. doi:10.1016/J.SOILDYN.2021.106832

Carvalho, A., Reis, C. and Vales, D. (2016). 'Source and high-frequency decay parameters for the Azores region for stochastic finite-fault ground motion simulations', *Bulletin of Earthquake Engineering*, 14, pp. 1885–1902. doi:10.1007/s10518-015-9842-y

Formisano, A. *et al.* (2021). 'Fem model calibration of experimental environmental vibration tests on two churches hit by L'Aquila earthquake', *International Journal of Architectural Heritage*, 15(1), pp. 113–131. doi:10.1080/15583058.2020.1719233

Fortunato, G., Funari, M.F. and Lonetti, P. (2017). 'Survey and seismic vulnerability assessment of the Baptistery of San Giovanni in Tumba (Italy)', *Journal of Cultural Heritage*, 26, pp. 64–78. doi: 10.1016/j.culher.2017.01.010. doi:10.1016/j.culher.2017.01.010

Funari, M.F., Hajjat, A.E., *et al.* (2021). 'A Parametric Scan-to-FEM Framework for the Digital Twin Generation of Historic Masonry Structures', *Sustainability 2021, Vol. 13, Page 11088*, 13(19), p. 11088. doi: 10.3390/SU131911088

Funari, M.F., Silva, L.C., *et al.* (2021). 'Real-time structural stability of domes through limit analysis: Application to St. Peter's Dome', *International Journal of Architectural Heritage,* 17(6), pp. 915–937. doi: 10.1080/15583058.2021.1992539

Funari, M.F. *et al.* (2022). 'A concurrent micro/macro FE-model optimized with a limit analysis tool for the assessment of dry-joint masonry structures', *International Journal for Multiscale Computational Engineering*, 20(5), pp. 65–85. Begell House. doi: 10.1615/intjmultcompeng.2021040212

Funari, M.F. *et al.* (2022). 'A solution for the frictional resistance in macro-block limit analysis of non-periodic masonry'. *Structures*, 43, pp. 847–859). Elsevier BV. doi: 10.1016/j.istruc.2022.06.072

Funari, M.F., Mehrotra, A. and Lourenço, P.B. (2021). 'A tool for the rapid seismic assessment of historic masonry structures based on limit analysis optimisation and rocking dynamics', *Applied Sciences (Switzerland)*, 11(3), pp. 1–22. doi: 10.3390/app11030942

Gaspar, J.L. *et al.* (2015). 'Chapter 4 Earthquakes and volcanic eruptions in the Azores region: geodynamic implications from major historical events and instrumental seismicity', *Geological Society, London, Memoirs*, 44(1), pp. 33–49. doi: 10.1144/M44.4

Gobbin, F., de Felice, G. and Lemos, J. v (2021). 'Numerical procedures for the analysis of collapse mechanisms of masonry structures using discrete element modelling', *Engineering Structures*, 246, p. 113047. doi: 10.1016/j.engstruct.2021.113047

Home | National Institute of Building Sciences (no date). https://www.nibs.org/ (Accessed: 27 August 2021)

Hoveidae, N., Fathi, A. and Karimzadeh, S. (2021). 'Seismic damage assessment of a historic masonry building under simulated scenario earthquakes: A case study for Arge-Tabriz', *Soil Dynamics and Earthquake Engineering*, 147, p.106732. doi:10.1016/J.SOILDYN.2021.106732

Karimzadeh, S. *et al.* (2020). 'Derivation of analytical fragility curves using SDOF models of masonry structures in Erzincan (Turkey)', *Earthquakes and Structures*, 18(2), pp. 249–261. doi:10.12989/eas.2020.18.2.249

Karimzadeh, S. *et al.* (2023). 'Backbone ground motion model through simulated records and XGBoost machine learning algorithm: An application for the Azores plateau (Portugal)', *In Earthquake Engineering & Structural Dynamics*, 53(2), pp. 668–693. Wiley. doi: 10.1002/eqe.4040

Karimzadeh, S. *et al.* (2024). 'Stochastic simulation of earthquake ground motions for the seismic assessment of monumental masonry structures: Source-based vs site-based approaches', *Earthquake Engineering & Structural Dynamics*, 53(1), pp. 303–330. doi: 10.1002/EQE.4012

Karimzadeh, S. and Lourenço, P.B. (2021). 'Stochastic Ground Motion Simulation of the 9th of July 1998 Faial Earthquake (Azores, North Atlantic)', *Earthquake Engineering Structural Dynamics*, 53(1), pp. 303–330. Wiley. doi: 10.1002/eqe.4012

Lourenço, N. *et al.* (1998). 'Morpho-tectonic analysis of the Azores Volcanic Plateau from a new bathymetric compilation of the area', *Marine Geophysical Research*, 20(3), p. 141

Lubliner, J. *et al.* (1989). 'A plastic-damage model for concrete', *International Journal of Solids and Structures*, 25(3), pp. 299–326. doi: 10.1016/0020-7683(89)90050-4

Marques, F.O. *et al.* (2014). 'The 1998 Faial earthquake, Azores: Evidence for a transform fault associated with the Nubia–Eurasia plate boundary?', *Tectonophysics*, 633, pp. 115–125. doi:10.1016/j.tecto.2014.06.024

Matias, L. *et al.* (2007). 'The 9th of July 1998 Faial Island (Azores, North Atlantic) seismic sequence', *Journal of Seismology*, 11, pp. 275–298

Motazedian, D. and Atkinson, G.M. (2005). 'Stochastic finite-fault modeling based on a dynamic corner frequency', *Bulletin of the Seismological Society of America*, 95(3), pp. 995–1010. doi: 10.1785/0120030207

Olafsson, S., Sigbjörnsson, R. and Einarsson, P. (1998). 'Estimation of source parameters and Q from acceleration recorded in the Vatnafjöll Earthquake in South Iceland', *Bulletin of the Seismological Society of America*, 88(2), pp. 556–563. doi:10.1785/BSSA0880020556

Olsen, K.B. and Mayhew, J.E. (2010). 'Goodness-of-fit criteria for broadband synthetic seismograms, with application to the 2008 Mw 5.4 Chino Hills, California, earthquake', *Seismological Research Letters*, 81(5), pp. 715–723. doi: 10.1785/gssrl.81.5.715

Pulatsu, B. *et al.* (2022). 'Probabilistic approach to assess URM walls with openings using discrete rigid block analysis (D-RBA)', *Journal of Building Engineering*, 61, p. 105269. doi: 10.1016/j.jobe.2022.105269

Rezaeian, S. and der Kiureghian, A. (2008). 'A stochastic ground motion model with separable temporal and spectral nonstationarities', *Earthquake Engineering & Structural Dynamics*, 37(13), pp. 1565–1584. doi: 10.1002/eqe.831

Rezaeian, S. and Xiaodan, S. (2014). 'Stochastic ground motion simulation'. Book chapter, Contributing office: Geologic Hazards Science Center, Publisher: Springer Berlin Heidelberg, 15 p.

Senos, M.L. *et al.* (1998). 'O terramoto do Faial de 9 de Julho de 1998', in *Proceedings do 1.° Simpósio de Meteorologia e Geofísica da APMG*, pp. 61–68, (In Portuguese).

Stepinac, M. *et al.* (2021). 'Damage classification of residential buildings in historical downtown after the ML5.5 earthquake in Zagreb, Croatia in 2020', *International Journal of Disaster Risk Reduction*, 56, p. 102140. doi: 10.1016/j.ijdrr.2021.102140

Valente, M. and Milani, G. (2016). 'Non-linear dynamic and static analyses on eight historical masonry towers in the North-East of Italy', *Engineering Structures*, 114, pp. 241–270. doi:10.1016/j.engstruct.2016.02.004

Yakut, A. and Yılmaz, H. (2008). 'Correlation of deformation demands with ground motion intensity', *Journal of Structural Engineering*, 134(12), pp. 1818–1828. doi: 10.1061/(ASCE)0733-9445(2008)134:12(1818). doi:10.1061/(ASCE)0733-9445(2008)134:12(1818

Zonno, G. *et al.* (2010). 'Assessing seismic damage through stochastic simulation of ground shaking: the case of the 1998 Faial earthquake (Azores Islands)', *Surveys in Geophysics*, 31, pp. 361–381. doi:10.1007/s10712-009-9091-1